Comprehensive Low-Field Mobility Modeling in Nano-Scaled SOI Channels

Z. Stanojević, O. Baumgartner, L. Filipović, and H. Kosina

Institute for Microelectronics, TU Wien, Gußhausstraße 27-29/E360, 1040 Wien, Austria

1 Abstract

We present a comprehensive computational toolset for low-field mobility modeling in nano-scaled SOI channels. The dimension-independent methodology allows us to treat planar devices (MOS, UTB) and non-planar ones (Bulk/SOI-FinFET, Nanowire-FET) on equal footing. The method involves combining a self-consistent Schrödinger-Poisson solution in the channel cross-section with a linearized Boltzmann transport model. Full numerical treatment of the scattering rates guarantees consistent results for all geometries. All scattering mechanisms relevant to the Si/SiGe material system are included and treated accurately.

2 Motivation

A myriad of SOI architectures have been proposed to replace traditional MOS technologies, including planar architectures, such as ultra-thin body (UTB) devices, and non-planar ones, such as bulk-FinFETs [1, 2] or SOI-FinFETs. Also, novel device ideas are emerging such as the junction-less FET [3]. In practice, one must be able to competitively rate different device designs and select the most appropriate one for the application at hand. Hence, a modeling framework able to perform these ratings consistently is highly desirable.

3 Modeling Tools

The presented toolchain is sketched in Fig. 1 as provided by the Vienna Schrödinger-Poisson (VSP) simulator [4] available within GTS Framework [5]. It features a self-consistent Schrödinger-Poisson (S/P) loop where all equations are discretized on an unstructured mesh and solved using fast state-of-the-art methods. A low-field mobility model based on the Kubo-Greenwood formula is run on the converged S/P-solution. Any number of scattering models may be included, the relevant ones for Si and SiGe being acoustic phonons (ADP), ionized impurities (IIS), surface roughness (SRS), alloy scattering, and inter-valley scattering (IVS) due to optical phonons.
SRS is treated using a novel method developed in our earlier work [6]. The method extends the existing SRS theory for planar devices to non-planar geometries of arbitrary shape ensuring consistency of results as demonstrated in Figs. 2 and 3. IIS uses a fully numerical approach where the Green's function is obtained numerically from the discretized Poisson equation using efficient sparse methods. This naturally includes geometry effects, inhomogeneous permittivity and dielectric screening.
The mobility calculation combines the scattering processes at the microscopic level by summing the scattering rates, rather than using Matthiessen's rule. The material anisotropy is fully taken into account by employing not only tensor-valued effective masses but also tensor-valued scattering rates.
Orientation and strain enter the model via the band structure through deformation potentials and valley anisotropies, respectively. A $\mathbf{k}\cdot\mathbf{p}$-based subband structure model is inserted into the simulation flow to account for variations of effective mass due to confinement or strain.

4 Results

We examine the properties of a junction-less (JL) device similar to the one reported in [3] and compare it to an inversion-mode device (Fig. 4). The influence of the various scattering processes in the JL device deviates considerably from the inversion-mode device (Fig. 5). The initial mobility is low in the JL case due to high IIS but increases as more carriers become available to screen the impurities. The JL device is far less affected by SRS compared to the inversion-mode device where SRS limits mobility at high inversion densities (Fig. 6).

5 Conclusion

We presented a versatile and efficient computational toolkit based on physical models for low-field mobility modeling in nano-scale devices. It enables differential analysis of devices which is crucial in the evaluation of novel device designs.

Acknowledgment

This work has been supported by the Austrian Science Fund through contracts F2509 and I841-N16.

References

[1] C. Auth *et al.*, *VLSIT* (2012), pp. 131–132.

[2] Z. Stanojevic *et al.*, *IEDM* (2013).

[3] J.-P. Colinge *et al.*, Nat Nano **5**, 225 (2010).

[4] O. Baumgartner *et al.*, J. Comput. Electron. (2013).

[5] http://www.globaltcad.com/en/products/vsp.html.

[6] Z. Stanojevic *et al.*, *Intl. Conf. on Simulation of Semiconductor Processes and Devices* (2013), pp. 352–355.

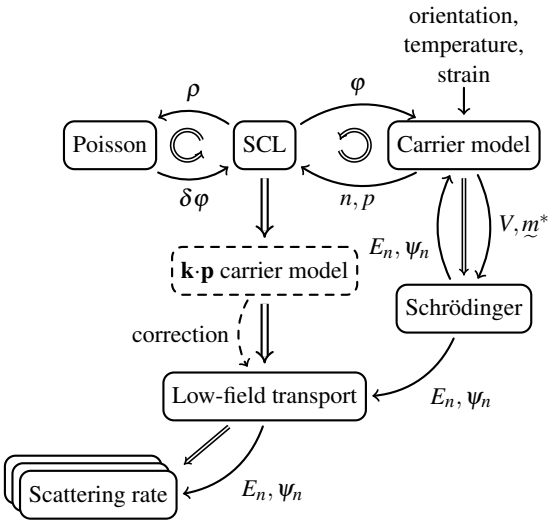

Fig. 1: Overall computational procedure; a self-consistent Schrödinger-Poisson loop (SCL) is run. The subband energies and wavefunctions of the converged solution are used to calculate scattering rates and mobilites. A **k**·**p**-based full-band carrier model may be inserted to provide corrections for subband effective masses and energies. Each box represents a model in the Vienna Schrödinger-Poisson framework highlighting its versatility – single arrows represent data flow, double arrows control flow.

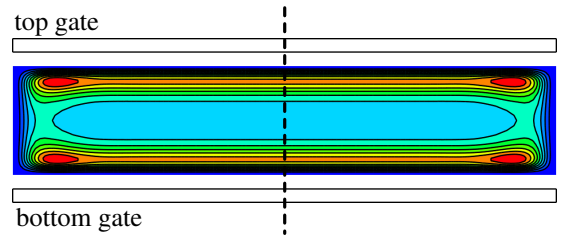

Fig. 2: Electron concentration in a finite-width double-gate UTB channel under gate bias resulting from a 2D Schrödinger-Poisson simulation; the same simulation is performed in 1D on a cut through the stack as indicated by the dashed line.

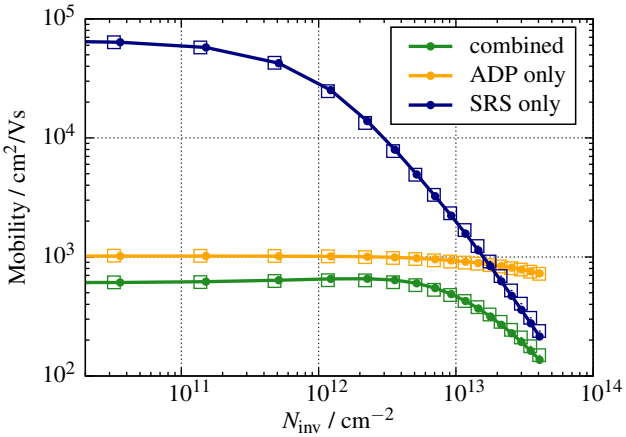

Fig. 3: Mobility curve for UTB channel from Fig. 2; lines – simulation on cut through device, open symbols – 2D analysis of finite-width channel; the curves are in perfect agreement, demonstrating the consistency between 1D and 2D simulations.

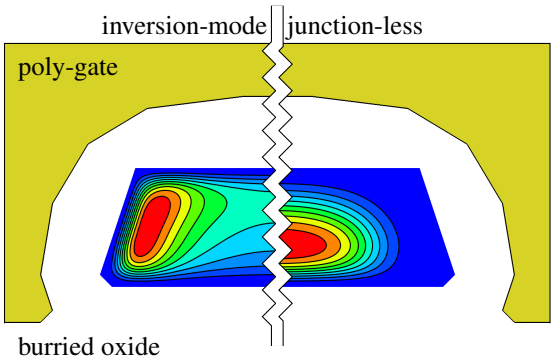

Fig. 4: Electron concentration in a pi-gate channel cross-section; left – inversion-mode device, right – junction-less device; both devices are biased above threshold. In the inversion-mode FET electrons are pushed towards the top and sidewalls while in the junction-less FET electrons remain centered.

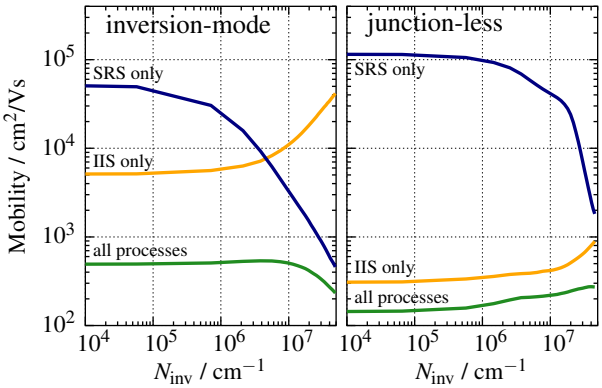

Fig. 5: Mobility curves for channel from Fig. 4; left – inversion-mode device, right – junction-less device; the dominant scattering processes are reversed for the two device types. In inversion-mode channels IIS is negligible and SRS dominates when the device is switched on. In the junction-less FET IIS is stronger by an order of magnitude, limiting the mobility, while SRS becomes effective at high densities only.

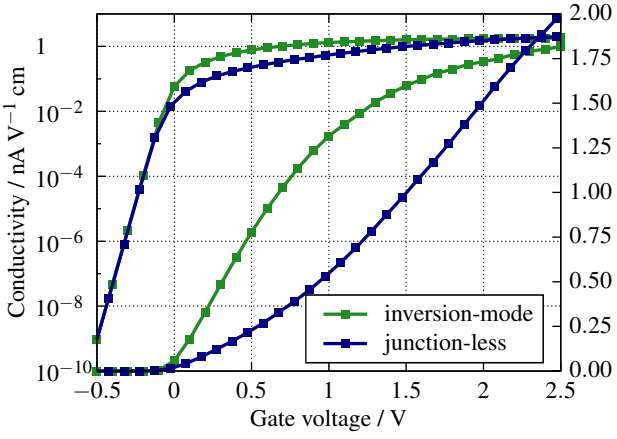

Fig. 6: Trans-conductivity for channels from Fig. 4; gate work-functions have been adjusted so that both the inversion-mode and the junction-less device have the same threshold voltage. In inversion-mode channels the conductivity saturates due to SRS. In junction-less devices conductivity is lower initially but shows no saturation.